Synthesis of Titanium Dioxide Nanoparticles with Mesoporous Anatase Wall and High Photocatalytic Activity

Tianyou Peng,*,†,‡ De Zhao,† Ke Dai,† Wei Shi,† and Kazuyuki Hirao§

Department of Chemistry, Centre of Nanoscience and Nanotechnology Research, Wuhan University, Wuhan 430072, China, State Key Laboratory of Coordination Chemistry, Nanjing University, China, and Fukui Institute for Fundamental Chemistry, Kyoto University, Japan

Received: November 15, 2004; In Final Form: January 3, 2005

Mesoporous titanium dioxide nanosized powder with high specific surface area and anatase wall was synthesized via hydrothermal process by using cetyltrimethylammonium bromide (CTAB) as surfactant-directing agent and pore-forming agent. The resulting materials were characterized by XRD, nitrogen adsorption, FESEM, TEM, and FT-IR spectroscopy. The as-synthesized mesoporous TiO_2 nanoparticles have mean diameter of 17.6 nm with mean pore size of 2.1 nm. The specific surface area of the as-synthesized mesoporous nanosized TiO_2 exceeded 430 m^2/g and that of the samples after calcination at 600 °C still have 221.9 m^2/g. The mesoporous TiO_2 nanoparticles show significant activities on the oxidation of Rhodamine B (RB). The large surface area, small crystalline size, and well-crystallized anatase mesostructure can explain the high photocatalytic activity of mesoporous TiO_2 nanoparticles calcined at 400 °C.

I. Introduction

Over the past decades, there has been increasing interest in the application of large surface area TiO_2 with nanosized powders or mesostructure for gas sensing, photocatalysts, photoelectrodes for photosplitting water, and solar energy conversion.[1−20] In these applications, the control of morphology, particle size, particle size distribution, phase composition, and porosity of TiO_2 is a vital factor in determining the properties of the final materials.[1−20] Among three crystalline phases of TiO_2, anatase exhibits the highest photocatalytic activity.[1] Nanosized anatase TiO_2 is the most attractive for these applications because of its large effective surface area which enhances the surface reactions. On the other hand, the smaller TiO_2 particles are also beneficial for the more effective photogenerated carriers separation and greater photocurrent, thus the higher photocatalytic and photoelectrical chemical conversion effencies.[2,10] Therefore, there are numerous investigations on the synthesis of anatase nanoparticles with sizes ranging from 5 nm to several micrometers and a variety of shapes for the photocatalysis and photoelectrode materials.[3−5] Among those reports, the sol−gel technique is the most frequently applied. Generally, the precipitates derived from the sol−gel process are amorphous;[6] the photocatalytic and photoelectrical conversion efficiencies of those obtained TiO_2 nanoparticles are not high enough for industrial purposes.[7] Hence, several methods have been reported to improve this situation, such as increasing the surface area, generation of defect structures to induce interfacial charge separation, and modification of the TiO_2 with metal or other semiconductors.[8−10]

Among those, mesoporous TiO_2 has attracted much attention because of its high surface-to-volume ratio, which is of great importance in photocatalysis, photosplitting water, and solar energy conversion.[11] Therefore, worldwide research activity based on mesoporous TiO_2 has ensued. Most of the proposed syntheses of mesoporous titania or titanium phosphates by precipitation depend on controlling the high reactivity of Ti(IV) by the addition of stabilizing agents. Uncontrolled hydrolysis and condensation lead to the formation of a dense inorganic network, generating poorly structured materials. The use of complex $Ti(OR)_{4-n}(AcAc)_n$ precursors, combined with phosphonate anionic surfactants in slightly acid medium, resulted in the first preparation of titania-based mesoporous oxide in 1995.[11] However, they are not pure TiO_2 because a significant amount of phosphorus still remained in these materials and underwent partial collapse of the mesopores during template removal by calcinations. The idea of addition of stabilizing reagents for controlling hydrolysis of $Ti(OR)_4$ is accepted extensively, for example, a tridentate ligand (triethanolamine) has been also used as stabilizer to product phosphorus-free wormlike, mesoporous TiO_2.[12] Blanchard et al. have also used protons in acid media to retard the rapid condensation and generate titanium mesostructured oxosulfates or mesoporous oxophosphates.[13,14] Moreover, surfactants,[15,16] triblock copolymer,[17] and many nonsurfactant organic compounds[18] as well as ultrasound-induced technology[10,19] have been successfully used to prepare mesoporous TiO_2. Solvent extraction or thermal treatment at low temperature was often used to remove the surfactants used in the preparation of mesoporous TiO_2.[12,15] However, the obtained amorphous and semicrystalline TiO_2 have insignificant photocatalytic activity.[20] Calcination at high temperature may not be beneficial for improving the photocatalytic activity as it results in the collapse of mesoporous framework and loss of surface area because of the crystallization of TiO_2 and the subsequent crystal growth.[21]

Since the anatase phase has a far higher photocatalytic and photoelectricalchemical conversion activity than amorphous and rutile TiO_2, it is still a challenge to synthesize mesoporous TiO_2 containing the high crystallization of anatase phase and large surface area.[1,22−24] To the best of our knowledge, there are few

* To whom correspondence should be addressed. E-mail: typeng@whu.edu.cn.
† Wuhan University.
‡ Nanjing University.
§ Kyoto University.

10.1021/jp044771r CCC: $30.25
Published on Web 02/24/2005

reports on the synthesis of TiO_2 nanoparticle with stable anatase mesostructures,[23] which has an advantage in relate to photocatalytic and photoelectrochemical properties. In this work, we apply a hydrothermal method to synthesize mesoporous anatase TiO_2 nanoparticles by using cetyltrimethylammonium bromide (CTAB) as a surfactant-directing agent and pore-forming agent in a facile and reproducible way. Hydrothermal treatment applied is helpful to crystallize mesoporous wall into anatase and stabilize the mesoporous structure. The obtained anatase TiO_2 nanoparticles with mesostructures show very high photocatalytic activity on the oxidation of Rhodamine B (RB) in air. The photocatalytic activity of the samples obtained in the present method exceeded that of commercial catalyst Degussa P25.

II. Experimental Section

Preparation and Characterization. All chemical reagents used in the present experiments were obtained from commercial sources as guaranteed-graded reagents and used without further purification. A typical synthesis process for the preparation of mesoporous TiO_2 nanoparticles with anatase wall is as follows: 1.1402 g $Ti(SO_4)_2$ was dissolved into 3.5 mL distilled water. The obtained solution was added into cetyltrimethylammonium bromide (CTAB) solution under stirring. The molar ration of $Ti(SO_4)_2$:CTAB:H_2O is 1:0.12:100. After stirring for 30 min, the resulting mixture was aged at room temperature for 12 h and then transferred into an autoclave at 100 °C for hydrothermal treatment. After 72 h, the resulting powders were cooled to room temperature, then recovered by centrifugation, washed with water and ethanol, and then dried at 120 °C overnight. To remove organic materials, ion-exchange treatment was performed by mixing the as-synthesized powders with a water and ethanol (molar ratio 1:1) solution of sodium chloride under stirring at 313 K for 5 h. The resulting solids were washed with water and ethanol and then dried at 120 °C overnight. The as-prepared samples were calcined at different temperatures for 6 h to improve crystallinity with a heating rate of 2 °C/min, respectively.

Field emission scanning electron microscopy images were obtained on a JSM-7400F (FESEM) electron microscope. Transmission electron microscopy images were obtained on a JEM-100X/II (TEM) and LaB6 JEM-2010(HT)-FEF (HRTEM) electron microscope. X-ray diffraction (XRD) patterns were obtained on XRD-6000 diffractometer using Cu Kα as radiation. The nitrogen adsorption and desorption isotherms at 77 K were measured on a Micrometrics ASAP 2010 system after samples were degassed at 120 °C. IR spectra on pellets of the samples mixed with KBr were recorded on a FTIR-8201PC spectrometer.

Measurement of Photocatalytic Activity. The photocatalytic activity experiments on the mesoporous TiO_2 nanoparticles for the oxidation of Rhodamine B (RB) in air were performed at ambient temperature. The UV source was a 300 W Hg lamp (100 mm long) with a maxium emission at approximately 365 nm, which was surrounded by a circulating water jacket (Pyrex) to cool the lamp. Typically, the aqueous RB/TiO_2 suspension was prepared by addition of TiO_2 (50 mg) to a 50 mL aqueous solution containing BR dye ($c_0 = 1.0 \times 10^{-5}$ M, pH 6.0). All runs were conducted at ambient pressure and temperature. The distance between the Hg lamp and the reactor was 30 cm for each experiment. The suspension was magnetically stirred before and during illumination. The suspension was mixed for 15 min in the dark (for the adsorption of dye onto the photocatalyst surface) and then the reaction mixture was exposed to the UV−vis light. After irradiation and removal of the TiO_2 particles by centrifugation, the residual RB was analyzed using a Shimadzu UV-240 spectrophotometer. For comparison, commercial catalyst Degussa P25 has also been conducted under identical experimental conditions.

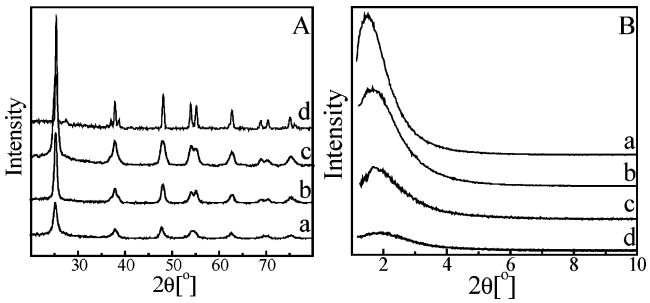

Figure 1. High-angle (A) and low-angle (B) XRD patterns of samples. (a) As-synthesized and calcined at (b) 400 °C, (c) 600 °C, (d) 800 °C.

TABLE 1: Summary of the Physicochemical Properties of Mesoprous TiO_2 Nanosized Powders

calcination temp (°C)	crystal size (nm)	S_{BET} (m^2/g)	mean pore size (nm)	total volume (cm^{-3}/g)
as-synthesized	2.3	438.3	2.1	0.56
400	3.1	317.5	2.5	0.61
600	4.2	221.9	2.8	0.50
800	7.5	71.5		0.32

III. Results and Discussion

The as-synthesized TiO_2 powders show broad anatase peaks (Figure 1Aa), indicating that the as-synthesized sample is anatase phase (JCPDS, No. 21-1272). After heat treatment, only peaks of anatase phase that become stronger and sharper are identified in Figure 1A (b and c). Average crystalline sizes calculated from the broadening of the (101) XRD peaks of the anatase phase are 2.3, 3.1, and 4.2 nm for the samples as-synthesized and calcined at 400 and 600 °C, respectively. Even for calcination at 800 °C for 6 h, the XRD pattern shows that the main crystal phase is still anatase, small peaks of rutile phase appeared, and the crystalline size increases to 7.5 nm (ref Table 1). The crystalline size of mesoporous samples changes slightly upon calcination, indicating the anatase grains in the mesostructures have a relatively high thermal stability. The stabilization of the anatase phase up to 800 °C can be attributed to the small size of inorganic domains. Zhang et al.[25] have shown that though rutile is the most stable phase for bulk materials, when a large amount of surface is present (such as for a nanoparticle smaller than 14 nm), anatase is stabilized, minimizing the total free energy of the system (bulk + surface).[26] Furthermore, it has been proved that the SO_4^{2-} anion and the acidic reaction condition (the initial pH of the mixture in the present systems is ∼0.8) in the hydrothermal condition can also retard the formation of rutile and the growth of crystal.[27] The thermal stabilities of mesostructures of the samples upon calcination are clearly revealed by the low-angle XRD patterns shown in Figure 1B. Except for the samples calcined at 800 °C, all patterns are similar and exbihit a single diffraction peak corresponding to *d* spacing of 5.56, 5.49, and 5.46 nm. This single strong diffraction peak in the low-angle region indicated the presence of mesostructure. Mesostructures with more or less regular diameter channel packed at random often display a single peak in low-angle XRD.[23] The considerable broadening and reduction in the intensity of pattern of the calcined samples, as well as the shifting of *d* spacing to lower distances, can be attributed to the partial shrinkage or collapse of the mesostructure upon calcination. A single broad peak is observed on low-angle XRD

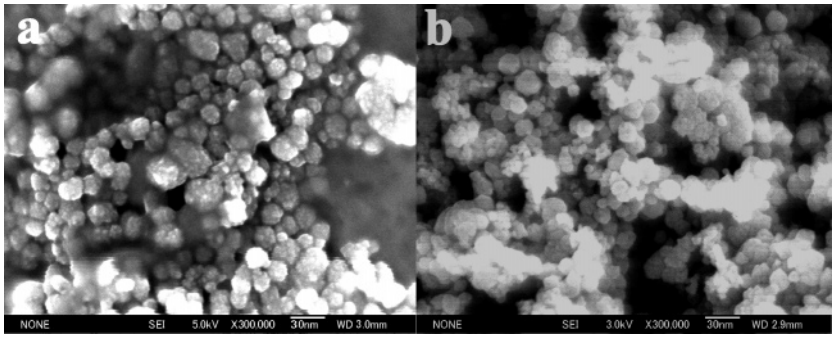

Figure 2. FESEM images of samples. (a) As-synthesized and (b) calcined at 400 °C.

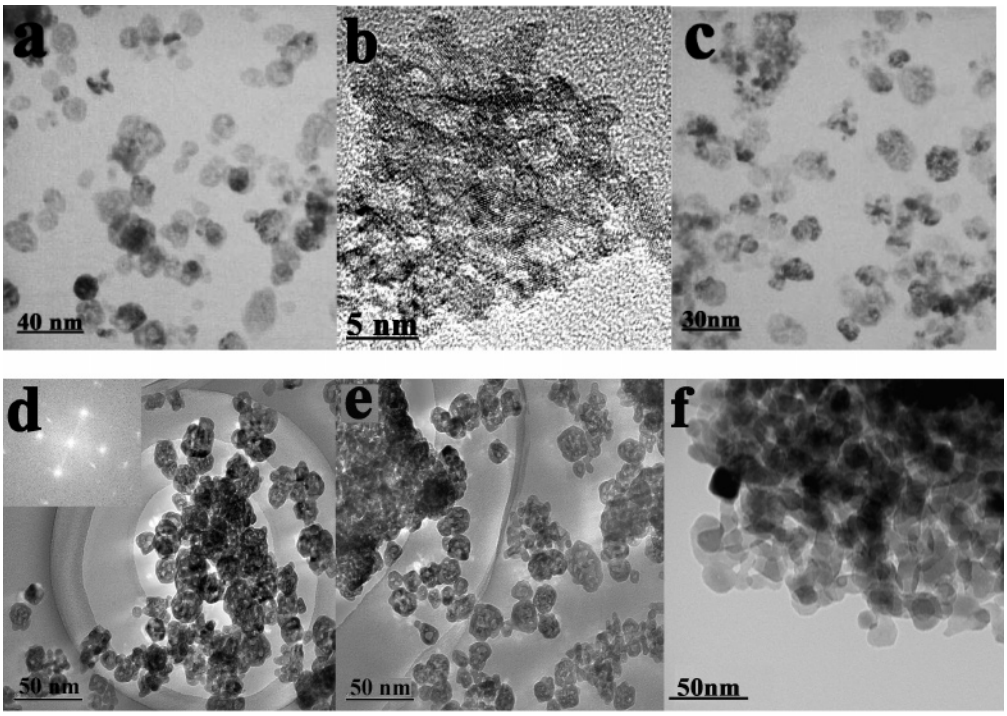

Figure 3. TEM and HRTEM images of samples. (a), (b) As-synthesized; (c), (d) calcined at 400 °C, (e) 600 °C, and (f) 800 °C.

patterns even for the sample calcined at 600 °C, suggesting the considerably high thermal stability of the mesostructure wall.

Figure 2 shows the FESEM images of the samples as prepared and calcined at 400 °C. As can be seen, the as-synthesized sample has a relative uniform particle diameter in the range of 7−27 nm with mean particle size of 17.6 nm. The surfaces of the nanoparticles are scraggy. This morphology may also contribute to the high surface area in the obtained samples. After calcinations at 400 °C, the mean particle size reduced to 15.7 nm, which can be ascribed to the shrinkage of the mesostructure upon calcinations. The more detailed microstructure of the nanoparticles can be seen from the TEM images (Figure 3) of the obtained samples. Except for the samples calcined at 800 °C, mesoporous structure without long-range order can be clearly observed in the obtained samples. The morphologies of pores and particles are not changed significantly upon heating to 600 °C, indicating that reconstruction or collapse does not occur drastically upon calcinations, although it can be observed that some particles have been cracked from the image of the sample calcined at 600 °C (Figure 3d). After calcinations at 800 °C, the powers ultimately change into nonporous particles with mean particle size of 18.4 nm (Figure 3f).

From the HRTEM of the as-synthesized mesoporous sample (Figure 3b), it can be clearly observed that the anatase phase has already formed in the mesoporous wall. The inserted electron diffraction patterns in Figure 3d also indicate that the crystallinity of anatase phase in the mesoporous wall is very high, which is consistent with XRD patterns of TiO_2 (inserted Figure 1 Ab). As can be seen from Figure 3a−e, the pore size and the wall thickness of the as-synthesized and calcined mesoporous TiO_2 nanoparticles are estimated to be 1.6−3.5 nm and 2.0−4.5 nm, respectively. The estimated wall thickness excellently coincides with the anatase nanodomains (2.3−4.2 nm, estimated according to the Scherrer equation) detected by high-angle XRD as described above, also implying that the crystallinity of anatase in the mesostructure of the as-synthesized sample is very good (Figure 3d). In previous work with PEO-based surfactants, Yang et al.[17] found that these crystalline domains were embedded in the mostly amorphous TiO_2 matrix. Cabrera et al. also reported 3 nm anatase in the mesoporous walls of a wormlike material.[12] In the present CTAB-templated TiO_2 system, however, the mesoporous wall is basically composed of nanocrystal with limited amount of amorphous titania matrix, implying that the hydrothermal treatment can efficiently crystallize the inorganic walls into anatase phase without destroying the mesostructure. After calcinations at 800 °C, the anatase crystallites begin to grow extensively and transform to rutile phase, then segregate from the mesostructures. Subsequently, the whole mesostructure is completely destroyed.

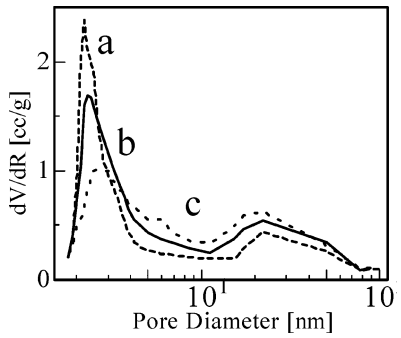

Figure 4. Barret−Joyner−Halenda (BJH) pore size distribution plots (inset) of samples. (a) As-synthesized and calcined at (b) 400 °C, (c) 600 °C.

The FT-IR spectra (Figure SI 1) of the obtained samples show that there are broad peaks at 3400 and 1638 cm^{-1}. It is believed that these broad peaks correspond to the surface-adsorbed water and hydroxyl groups.[16,24] The decrease in the intensities of these peaks in the spectrum of the samples with increased calcination temperature confirms the diminishing of the surface-adsorbed water and hydroxyl groups. The IR-absorption band at 2924 and 2854 cm^{-1} (ν_{CH3} and ν_{CH2}) as well as 1350−1500 cm^{-1} (δ_{CH}) in the as-synthesized TiO_2 can be attributed to the characteristic frequencies of residual CTAB, which is not removed completely by the ion-exchange processes.[16,24] The peaks at 460, 620, and 910 cm^{-1} in the range of 400−1000 cm^{-1} are contributions from the anatase phase.[16,24,26] The intensities of this large band of the as-synthesized sample enhanced insignificantly upon thermal treatment, implying that the anatase phase has already formed in the as-synthesized samples.

All samples show isotherms of type IV N_2 adsorption−desorption isotherms (Figure SI 2) with hysteresis loops, clearly indicating the mesoporous nature of TiO_2, but the considerable hysteresis loop at high relative pressures confirms that the mesopores in the samples were not too regular. While considering that the mesopores and nanoparticles coexist in the obtained samples, it would be reasonable to think that the hysteresis loops can be attributed to the total contribution of both intraparticle pores and interparticle pores. The pore size distribution (Figure 4) of the as-synthesized sample determined from BJH desorption isotherm shows a bimodal pore size distribution consisting of smaller fine (1.8−6.0 nm) with intraparticle pores and larger (15−70 nm) interparticle pores. The intraparticle pore size is in the range of 1.8−6.0 nm with mean pore diameter distribution at 2.1 nm, as was observed from HRTEM (Figure 3). Moreover, the grain size becomes larger and mesopores begin to partly collapse upon calcinations, which results in the intraparticle pore size shifting to a larger mesoporous region. The sample calcined at 400 °C still maintains relatively narrow intraparticle pore size distribution. After calcination at 600 °C, the intraparticle pore becomes weaker. It can be ascribed to the collapse of the intraparticle pores and the crystal growth. However, the pore size distribution of the interparticle pores just changed slightly upon calcination, indicating that the interparticle pores as well as the particle sizes changed insignificantly. The BET specific surface areas and pore volumes of the samples are summarized in Table 1. The relative high surface area (221 m^2/g) of the sample calcined at 600 °C confirms that the framework of mesoporous TiO_2 is relatively stable. Moreover, the large reduction of the surface area of the samples calcined at 800 °C shows substantial pore damage and crystallite growth or sintering, as indicated in Figure 3 and Table 1.

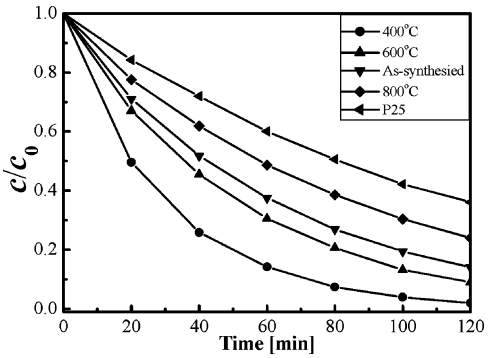

Figure 5. The photocatalytic properties of mesoporous TiO_2 samples as prepared and calcined at different temperature as well as the P25 nanoparticles (RB, $c_0 = 1.0 \times 10^{-5}$ M, pH 6.0) under UV-light radiation with increasing irradiation time.

The photocatalytic activity of the obtained mesoporous TiO_2 nanopowders was detected by the degradation of Rhodamine B (RB) aqueous solution under UV irradiation. For comparison, the photocatalytic activity of commercial nonporous photocatalyst P25 was also measured under identical conditions. The results clearly demonstrate the superior performance of the obtained samples, as shown in Figure 5. It can be seen that the degradation of RB is increased upon prolonging the irradiation time. Longer time irradiation obviously causes more degradation of RB. The optimum reactivity is observed at the sample calcined at 400 °C, which causes 97% RB to be degraded after 2 h irradiation. The photoactivity gradually decreased with further increases in calcination temperature. However, all of the materials show better activity than Deguess P25 TiO_2.

The surface areas and pore sizes of the obtained samples allow for comparison with previous work: Antonelli et al.[11] (200 m^2 g^{-1}, 3.2 nm calcined, at 400 °C), Stone et al.[15] (300 m^2 g^{-1}, 2.4 nm, calcined at 400 °C), and Blanchard et al.[14] (350 m^2 g^{-1}, 2.1 nm, calcined at 350 °C). The high surface area of the obtained samples can be attributed to the hydrothermal treatment, which is beneficial for crystallizing porous wall into anatase and effectively increasing its thermal stability, thus preventing the mesopores from collapsing. The obtained materials present some useful characteristics for the photocatalysis, such as the large and accessible pore surfaces, small crystal size, high crystallization of anatase mesostructures, and so forth. Therefore, it is worthy to discuss the reason of the high photocatalytic activity of the obtained samples here.

For effective degradation, the organic material should be preconcentrated at the semiconductor surface to effectively trap the respective reactive radicals. Generally, stable mesostructures allow rapid diffusion of various reactants and products during photocatalytic reaction and enhance the speed of photocatalytic reactions and also can offer more active sites to adsorb water and hydroxyl groups. The surface-adsorbed water and hydroxyl groups acted as photoexcited hole traps on the catalyst surface and produced hydroxyl radicals, which are powerful oxidants in degrading organics.[10] However, according to our experiment, the concentration of substrate at the semiconductor surface is not the only factor that influences the photoactivity. It can be found from Figure 5 that the photocatalytic activity increased when the calcination temperature increased to 400 °C. Compared with the as-synthesized sample, the sample calcined at 400 °C possesses reduced surface area but a more excellent crystallinity, as indicated in Figure 1 and Table 1. Therefore, we think that the degree of crystallinity also played a major role in the photoactivity of TiO_2. Previous researchers showed that polycrystalline samples of TiO_2 have high photoproduction rates of

SCHEME 1: Idealized Formation Model of Mesoporous TiO_2 Nanopowders

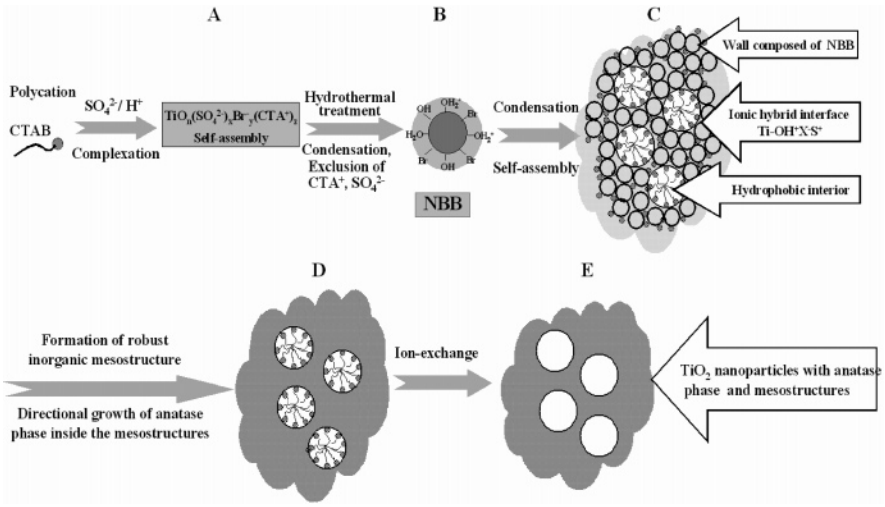

dihydrogen as compared with amorphous forms.[28] Ohtani et al. determined that, for constant particle size, the photocatalytic activity of TiO_2 increased linearly with the fractional crystallinity of anatase.[20] Apparently, crystallinity and photoactivity are inextricably linked. The photoactivity slightly reduced when the calcination temperature increased from 400 to 600 °C. The slow activity reduction showed by samples heated at 600 °C may be attributed to the extensive decreases of specific surface area, as we described in Table 1. Moreover, the photodegradation activity is reduced considerably for the samples calcined at 800 °C. It is commonly accepted that smaller crystalline size means more powerful redox ability because of the quantum-size effect.[2,10,29,30] Moreover, the smaller crystalline sizes are also beneficial for the separation of the photogenerated hole and electron pairs. These features should slow the rate of $e^- - h^+$ recombination and increase the photocatalytic activity. Therefore, it would be reasonable to conclude that the high photocatalyitc activity of the mesoporous TiO_2 nanoparticles calcined at 400 °C can be attributed to the high surface area, the well-crystallized anatase mesostructures, and the smaller crystalline size. Further studies are necessary to clarify the effects of the surface area, microstructure, and crystalline composition of TiO_2 on the photocatalytic activity.

In many papers along with the titania/CTAB literature, the ordered mesophase or mixed mesophase has been formed.[12−16] The investigation of phase behavior for $TiOSO_4$/CTAB composite showed that the initial step is a rapid formation of an ordered mesophase with a low degree of condensation, depending on the surfactant and the ionic strength of the solution.[13,14] However, there is no ordered mesophase observed in the present system, and this can be attributed to the obvious differences between our system and the previous reports, such as the much larger amount of SO_4^{2-}, the lower concentration of surfactant and reactants, and the different pH, which would be vital factors during the formation of ordered mesophase.[13] So, a model accounting for those differences for the formation of the present specific inorganic framework was developed, which is similar, to some extent, with the model presented by Sanchez et al.[16]

According to Blanchard et al.,[14] before the hydrothermal treatment, the SO_4^{2-} groups first complex the titanium polycations (e.g., $[Ti(OH)(H_2O)_5]^{3+}$, $[TiO(H_2O)_5]^{2+}$ that are present at low pH). The negatively charged inorganic species thus produced by this complexation reacts with the CTAB cationic surfactant. However, because of the lower concentration of surfactant in the present system compared with the previous reports,[13−16] the extended condensation is retarded by the lower pH condition (initial pH is 0.8 in the present system). Therefore, only highly flexible organic−inorganic self-assemblies at a low degree of condensation may be formed in the present stage (Scheme 1, Stage A). At the initial stages of the hydrothermal process, for the titanium-based hybrid self-assemblies described above, the SO_4^{2-} ions would be expelled during the framework condensation while oxo or additional hydroxo bridges are formed between the titanium centers.[13,14] The SO_4^{2-} density and thus the charge density are therefore expected to decrease during the condensation of the inorganic framework. The removal of SO_4^{2-} during the condensation induces the expulsion of CTAB molecules from the pores to maintain the overall charge neutrality of the mesophase. A low-condensed hybrid mesostructure will grow as positive Ti-oxo-based nanobuilding blocks (NBB), which are composed of $Ti-OH_2^+$ groups and bromide ions, coordinated or not to Ti surface atoms (Scheme 1, stage B).[16] Scanchez et al. have described that the titanium species can undergo a partial condensation at an appropriate low pH, generating $TiO_{2-x/2}(OR, OH, Cl)_x$ ($x = 0.2-0.5$). Discrete NBB have been characterized in titanium alkoxide/alcohol/acid media by small-angle X-ray scattering.[31] In acidic media, these NBB are compact hydrophilic clusters with ca. 2-nm gyration radius, depending on pH.[32] Because $pH < pH_{iep}$ TiO_2, surface hydroxy or $-OH_2^+$ groups are present.[31] Thus, the solid obtained from hydrothermal treatment should present an $I^+X^-S^+$ type of interface[29] ($X^- = Br^-$). Therefore, we think similar discrete hydrophilic nanosized Ti-oxo NBB are formed prior to the development of the mesostructured hybrid phase in the present system (Scheme 1, stage B).[16,32,33]

As further condensation of the inorganic framework, more and more surfactant will be expelled from the Ti-ox NBB. Therefore, the relative concentration of the surfactant in the mixture will be gradually increasing, which may result in the formation of disordered liquid-crystal-like mesophases composed of preformed titania nanobuilding blocks (NBB), which are self-assembled within a liquid-crystal-like mesophase, around micelle assemblies (Scheme 1, stage C). Once the final volume is reached and the liquid-crystal phase is kinetically "frozen", the systems are able to reorganize, to optimize the ionic, colloidal, and van der Waals interactions between the inorganic NBB and the micelles. This mesostructure is hydrothermally reinforced to assist inter-NBB condensation, leading to robust inorganic mesostructure. In general, the strong coordination capability with Ti−O octahedron leads to the

following two results: first, it is favorable to the formation of stable mesoporous structure between negative charge Ti(IV) species−SO_4^{2-}complex and cationic template microcells; second, the presence of a large amount of SO_4^{2-} prevents the Ti(IV) species from quick hydrolysis and crystallization to bulk titania. At the same time, upon further condensation between NBB, the directional growth of anatase phase inside the NBB may also occur at this stage. On the other hand, because of the present closed experiment, in which the initial reactants and the final products were present at pH < 1 environment as well as the lower concentration of surfactant, we can only obtain the nanoparticles with disordered mesostructure rather than ordered mesophase (Scheme 1, stage D). Ion exchange of the products leads to high surface area, TiO_2 nanoparticles with anatase phase wall in the mesoporous domains (Scheme 1, stage E).

IV. Conclusion

In summary, mesoporous TiO_2 nanosized powders with high surface area and stable anatase wall were prepared by using CTAB as directing agent and poreforming agent via a hydrothermal processes. Most organic compounds in mesoporous nanosized powders could be removed by anion-exchange process. Hydrothermal treatment crystallized powders into anatase without destroying the mesostructure and increased the surface area of the powders significantly. These mesoporous materials with anatase wall can be applied promisingly in photocatalysis and photoelectricalchemical application. The obtained mesoporous TiO_2 nanopowders exhibit higher photocatalytic activity than the commercial nonporous photocatalyst P25. We conclude that the high photocatalytic activity of the calcined mesoporous TiO_2 nanosized powders is related to its larger surface area, its smaller anatase crystalline size, and the high crystallinity of the high thermal stable mesostructure TiO_2.

Acknowledgment. The work described in this paper was partially supported by the Natural Science Fund of Hubei Province, China.

Supporting Information Available: FT-IR spectra and N_2 adsorption−desorption isotherms of samples (Supporting Information Figures S1−S2, in PDF format). This material is available free of charge via the Internet at http://pubs.acs.org.

References and Notes

(1) Ovenstone, J.; Yanagisawa, K. *Chem. Mater.* **1999**, *11*, 2770.
(2) Zhang, Z.; Wang, C. C.; Zakaria, R.; Ying, J. Y. *J. Phys. Chem. B* **1998**, *102*, 10871.
(3) Morrison, P. W.; Raghavan, R., Jr.; Timpone, A. J.; Artelt, C. P.; Pratsinis, S. E. *Chem. Mater.* **1997**, *9*, 2702.
(4) Murakami, Y.; Matsumoto, T.; Takasu, Y. *J. Phys. Chem. B* **1999**, *103*, 1836.
(5) Komarneni, S.; Rajha, T. K.; Katsuki, H. *Mater. Chem. Phys.* **1999**, *61*, 503.
(6) Wang, C. C.; Ying, J. Y. *Chem. Mater.* **1999**, *11*, 3113.
(7) Kwon, Y. K.; Song, K. Y.; Lee, W. L.; Choi, G. J.; Do, Y. R. *J. Catal.* **2000**, *191*, 192.
(8) Rusu, C. N.; Yates, J. T. *Langmuir* **1997**, *13*, 4311.
(9) Litter, M. I.; Navio, J. A. *J. Photochem. Photobiol., A: Chem.* **1996**, *98*, 171.
(10) Yu, J. C.; Zhang, L. C.; Yu, J. G. *Chem. Mater.* **2002**, *14*, 4647.
(11) Antonelli, D. M.; Ying, J. Y. *Angew. Chem., Int. Ed. Engl.* **1995**, *34*, 2014.
(12) Cabrera, S.; El-Haskouri, J.; Beltran-Portier, A.; Beltran-Portier, D.; Marcos, A. D.; Amoros, P. *Solid State Sci.* **2000**, *2*, 513.
(13) Linden, M.; Blanchard, J.; Schacht, S.; Schunk, S.; Schuth, F. *Chem. Mater.* **1999**, *11*, 3002.
(14) Blanchard, J.; Schuth, F.; Trens, P.; Hudson, M. *Microporous Mesoporous Mater.* **2000**, *39*, 163.
(15) Stone, V. F., Jr.; Davis, R. J. *Chem. Mater.* **1998**, *10*, 1468.
(16) Soler-IIIia, G. de. A. A.; Louis, A.; Sanchez, C. *Chem. Mater.* **2002**, *14*, 750.
(17) Yang, P. D.; Zhao, D. Y.; Margolese, D. I.; Chmelka, B. F.; Stucky, G. D. *Nature* **1998**, *396*, 152.
(18) (a) Wang, C.; Li, Q.; Wang, R. D. *Mater. Lett.* **2004**, *58*, 1424. (b) Zheng, J. Y.; Pang, J. B.; Qiu, K. Y.; Wei, Y. *J. Mater. Chem.* **2001**, *11*, 3367.
(19) Yu, J. C.; Yu, J. G.; Ho, W. K.; Zhang, L. Z. *Chem. Commun.* **2001**, 1942.
(20) Ohtani, B.; Ogawa, Y.; Nishimoto, S. I. *J. Phys. Chem. B* **1997**, *101*, 3746.
(21) Elder, S. H.; Gao, Y.; Li, X.; Liu, J.; McCready, D. E.; Windisch, C. F. *Chem. Mater.* **1998**, *10*, 3140.
(22) Huang, L. M.; Li, Q. Z. *Chem. Lett.* **1999**, *28*, 829.
(23) (a) Wang, Y. D.; Ma, C. L.; Sun, X. D.; Li, H. D. *Mater. Lett.* **2002**, *54*, 359. (b) Peng, T. Y.; Hasegawa, A.; Qiu, J. R.; Hirao, K. *Chem. Mater.* **2003**, *15*, 2011 and the references therein.
(24) Yu, J. M.; Zhang, L. Z.; Zheng, Z.; Zhao, J. C. *Chem. Mater.* **2003**, *15*, 2280.
(25) Zhang, H.; Banfield, J. F. *J. Mater. Chem.* **1998**, *8*, 2073.
(26) Crepaldi, E. L.; Soler-IIIia, G. J. de A. A.; Grosso, D.; Cagnol, F.; Ribot, F. *J. Am. Chem. Soc.* **2003**, *125*, 9770.
(27) (a) Wu, M.; Lin, G.; Chen, D.; Wang, D.;. He, G.; Feng, S.; Xu, R. *Chem. Mater.* **2002**, *14*, 1974. (b) Izumi, F. *Bull. Chem. Soc. Jpn.* **1978**, *51*, 771.
(28) Kallala, M.; Sanchez, C.; Cabane, B. *Phys. Rev. E* **1993**, *48*, 3692.
(29) Davidson, R. S.;. Morrison, C. L.; Abraham, J. *J. Photochem.* **1994**, *24*, 27.
(30) Hoffmann, M. R.; Martin, S. T.; Choi, W. Y.; Bahnemann, D. W. *Chem. Rev.* **1995**, *95*, 69.
(31) Lin, J.; Yu, J. C.; Lo, D.; Lam, S. K. *J. Catal.* **1999**, *183*, 368.
(32) Blanchard, J.; Ribot, F.; Sanchez, C.; Bellot, P. V.; Trokiner, A. *J. Non-Cryst. Solids* **2000**, *265*, 83.
(33) Yoon, R. H.; Salman, T.; Donnay, G. *J. Colloid Interface Sci.* **1979**, *70*, 483.